

## Article

# SNP-Associated Substitutions of Amino Acid Residues in the dNTP Selection Subdomain Decrease Pol $\beta$ Polymerase Activity

Olga A. Kladova <sup>1,\*</sup>, Timofey E. Tyugashev <sup>1</sup>, Aleksandr A. Miroshnikov <sup>2</sup>, Daria S. Novopashina <sup>1</sup>,  
Nikita A. Kuznetsov <sup>1,2</sup> and Aleksandra A. Kuznetsova <sup>1,\*</sup>

<sup>1</sup> Institute of Chemical Biology and Fundamental Medicine, Siberian Branch of Russian Academy of Sciences, 630090 Novosibirsk, Russia; tyugashev@niboch.nsc.ru (T.E.T.); danov@niboch.nsc.ru (D.S.N.); nikita.kuznetsov@niboch.nsc.ru (N.A.K.)

<sup>2</sup> Department of Natural Sciences, Novosibirsk State University, 630090 Novosibirsk, Russia; a.miroshnikov@g.nsu.ru

\* Correspondence: kladova@niboch.nsc.ru (O.A.K.); sandra-k@niboch.nsc.ru (A.A.K.)

**Abstract:** In the cell, DNA polymerase  $\beta$  (Pol $\beta$ ) is involved in many processes aimed at maintaining genome stability and is considered the main repair DNA polymerase participating in base excision repair (BER). Pol $\beta$  can fill DNA gaps formed by other DNA repair enzymes. Single-nucleotide polymorphisms (SNPs) in the *POLB* gene can affect the enzymatic properties of the resulting protein, owing to possible amino acid substitutions. For many SNP-associated Pol $\beta$  variants, an association with cancer, owing to changes in polymerase activity and fidelity, has been shown. In this work, kinetic analyses and molecular dynamics simulations were used to examine the activity of naturally occurring polymorphic variants G274R, G290C, and R333W. Previously, the amino acid substitutions at these positions have been found in various types of tumors, implying a specific role of Gly-274, Gly-290, and Arg-333 in Pol $\beta$  functioning. All three polymorphic variants had reduced polymerase activity. Two substitutions—G274R and R333W—led to the almost complete disappearance of gap-filling and primer elongation activities, a decrease in the deoxynucleotide triphosphate-binding ability, and a lower polymerization constant, due to alterations of local contacts near the replaced amino acid residues. Thus, variants G274R, G290C, and R333W may be implicated in an elevated level of unrepaired DNA damage.

**Keywords:** DNA repair; DNA polymerase beta; single-nucleotide polymorphism; enzymatic activity



**Citation:** Kladova, O.A.; Tyugashev, T.E.; Miroshnikov, A.A.; Novopashina, D.S.; Kuznetsov, N.A.; Kuznetsova, A.A. SNP-Associated Substitutions of Amino Acid Residues in the dNTP Selection Subdomain Decrease Pol $\beta$  Polymerase Activity. *Biomolecules* **2024**, *14*, 547. <https://doi.org/10.3390/biom14050547>

Academic Editors: Lorenzo Manti and Alexandros Georgakilas

Received: 27 March 2024

Revised: 18 April 2024

Accepted: 30 April 2024

Published: 2 May 2024



**Copyright:** © 2024 by the authors. Licensee MDPI, Basel, Switzerland. This article is an open access article distributed under the terms and conditions of the Creative Commons Attribution (CC BY) license (<https://creativecommons.org/licenses/by/4.0/>).

## 1. Introduction

Effects of various environmental factors acting on the cell constantly lead to damage to genetic information encoded in DNA [1]. Such lesions can cause mutations in the genome, which means defects in the integrity of the genetic information [2–5]. To maintain genome stability, living organisms have several DNA repair systems that preserve their original sequence [6,7]. One such system is base excision repair (BER), which involves the action of many enzymes [8]. The first to find and recognize a base lesion are DNA glycosylases, which remove the damaged base [9–11]. The resulting apurinic/apyrimidinic (AP) site can then be hydrolyzed by AP endonuclease 1 [12,13]. The next enzyme acting in this pathway is DNA polymerase  $\beta$  (Pol $\beta$ ) [14]. The latter is considered the main repair DNA polymerase whose main function is to fill the gaps in DNA (formed after the action of AP endonuclease 1) with complementary deoxynucleotide triphosphates (dNTPs) via the short-patch BER pathway [15]. Under certain conditions, Pol $\beta$  can continue the synthesis by generating longer DNA fragments with strand displacement via the long-patch pathway [16,17].

Pol $\beta$  is a small protein with a mass of 39 kDa. The enzyme has two structural domains: dRP-lyase and nucleotidyl transferase [15,18,19]. The nucleotidyl transferase domain can be functionally divided into several subdomains: the DNA-binding subdomain, the nucleotidyl transferase subdomain, and the subdomain of dNTP selection. One of the

most important functions of Pol $\beta$  is to fill a gap in DNA with a complementary nucleotide monophosphate (dNMP). The correct choice of complementary dNTP is necessary to prevent mutations. The interactions of the dNTP selection domain (amino acid residues [aa] 269–335) with incoming dNTP are critical for the selection of a complementary dNTP to incorporate.

Amino acid residues of Pol $\beta$  form many contacts with substrates (DNA and dNTP); disruption of the extensive network of the interactions because of substitutions of amino acid residues in the enzyme can result in changes in the activity of the enzyme. Such amino acid substitutions can arise due to the occurrence of natural single-nucleotide polymorphisms (SNPs) in the genome [20]. It is known that the genes of DNA repair enzymes contain many SNPs, some of which considerably affect their function [21,22]. Most SNPs found in the *POLB* gene are localized to introns or do not lead to a change in the functional class of an affected amino acid residue. Analysis of various polymorphisms has made it possible to detect various SNPs that alter the class of the amino acid residue in the enzyme (missense mutations) and can therefore affect its function [23]. In the dNTP selection subdomain, there are amino acid substitutions (described in databases) caused by SNPs found in patients with various tumors (Table 1).

**Table 1.** Occurrence of amino acid substitutions in the dNTP selection subdomain of Pol $\beta$  for various types of tumors.

aa Substitution	HIVE Biochemistry ( <a href="https://hive.biochemistry.gwu.edu">https://hive.biochemistry.gwu.edu</a> accessed on 21 February 2021)	COSMIC ( <a href="https://cancer.sanger.ac.uk">https://cancer.sanger.ac.uk</a> accessed on 21 February 2021)	cBioportal ( <a href="https://www.cbioportal.org">https://www.cbioportal.org</a> accessed on 21 February 2021)
L270P		Hepatocellular carcinoma	Hepatocellular carcinoma
G274V		Malignant melanoma	Cutaneous melanoma
I277V		Uterine endometrioid carcinoma	Uterine cancer
K280N	Lung squamous cell carcinoma	Squamous cell lung carcinoma	Lung cancer
N281S	Hepatocellular carcinoma		Blastoma
M282I	Cervix squamous cell carcinoma	Squamous cell cervical carcinoma	Cervical cancer
R283S	Breast carcinoma		
A284V		Uterine endometrioid carcinoma	Uterine cancer
A286S			Liver cancer
A286V	Colon adenocarcinoma		
E288K	Breast carcinoma	Invasive ductal carcinoma	Breast cancer
G290D			Uterine cancer
F291L	Upper aerodigestive tract squamous cell carcinoma		
Y296D	Small cell lymphocytic lymphoma		
R299C	Colon adenocarcinoma		
R299S	Upper aerodigestive tract squamous cell carcinoma	Head and neck squamous cell carcinoma	
P300L	Malignant melanoma		
G305E	Metaplastic breast carcinoma		Breast cancer
A307T	Malignant melanoma		
E309K	Transitional cell carcinoma		
P310L	Malignant melanoma		
D314Y	Acute myeloid leukemia		Hematological cancer

Table 1. Cont.

aa Substitution	HIVE Biochemistry ( <a href="https://hive.biochemistry.gwu.edu">https://hive.biochemistry.gwu.edu</a> accessed on 21 February 2021)	COSMIC ( <a href="https://cancer.sanger.ac.uk">https://cancer.sanger.ac.uk</a> accessed on 21 February 2021)	cBioportal ( <a href="https://www.cbioportal.org">https://www.cbioportal.org</a> accessed on 21 February 2021)
K317I	Malignant melanoma		
I319V	Glioma	Astrocytoma	Malignant glioma
D321N	Colon adenocarcinoma		
Y322C	Colon adenocarcinoma		Melanoma
W325L	Malignant melanoma	Cutaneous melanoma	
R328Q	Malignant melanoma		
D332N	Merkel cell carcinoma		
R333W	Prostate adenocarcinoma		Prostate cancer
R333Q	Cecum adenocarcinoma	Colon adenocarcinoma	Colorectal cancer

For some SNPs located in the dNTP selection subdomain, the effect on enzymatic properties of Pol $\beta$  is known. For example, variant Glu288Lys has been reported to have lower fidelity of dATP incorporation into single-nucleotide (1-nt) gap-containing DNA [24]. At the same time, dissociation constants  $K_d$ , polymerase reaction rate constant  $k_{obs}$ , and rate of product release  $k_{ss}$  are similar between the Pol $\beta$  variant and wild type (WT) Pol $\beta$ . The Lys289Met variant more frequently attaches dCTP opposite cytidine in DNA, thereby showing poor discrimination of dNTPs during the transferase reaction [25,26]. It has been demonstrated that the rate constant of dNTP incorporation into 1-nt gap-containing DNA in this variant is considerably lower than that of WT Pol $\beta$ . Meanwhile, the dissociation constant  $K_d$  is virtually the same. The polymorphic variant containing the Glu295Lys substitution does not possess polymerase activity, thereby leading to the emergence of unfilled gaps in DNA. This mutant of Pol $\beta$  has been detected in patients with gastric carcinoma [27].

We recently analyzed known SNPs in the *POLB* gene that lead to a change in the class of an amino acid residue and can therefore disrupt the function of the amino acid residue [23]. As a result of the analysis, 196 substitutions of amino acid residues were identified, among which 33 substitutions were located in the dNTP selection subdomain. They were ranked according to the possible negative impact on the functioning of the Pol $\beta$  enzyme. In the dNTP selection subdomain, several substitutions were found with a high risk of impairment of the enzyme's action, including substitutions G274R, G290C, E316K, P330L, R333Q, and R333W, located at the C terminus of the enzyme (Figure 1). The role of some of these amino acid residues has already been discussed in the literature [28,29]. Unstudied SNP variants G274R, G290C, and R333W were selected for further analysis.

Gly-274 is a conserved residue located between DNA helices M and N in a protein region undergoing considerable conformational rearrangements [30]. The substitution of Gly-274 with Val has been identified in melanoma patients (databases COSMIC and cBioportal). Gly-290 is located at a distance from the active center of the enzyme; in the binary complex with DNA and in the ternary complex with DNA and dNTP, this residue becomes closer to DNA [15,18,31]. Arg-333 is located in a poorly structured region of the C-terminal tail [18]. Despite the distal localization from the active center, it is known that some functional mutations of the amino acid residue at position 333 induce almost complete inactivation of the enzyme [29]. The current work presents a study about the enzymatic properties of SNP-associated Pol $\beta$  variants G274R, G290C, and R333W, and the influence of these amino acid substitutions on local contacts in the enzyme.

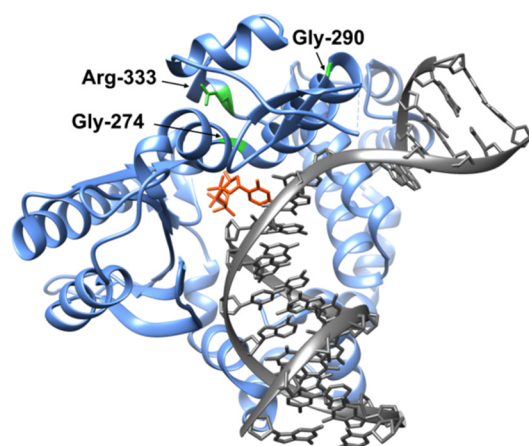


**Figure 1.** The ternary complex of Pol $\beta$  with DNA containing a 1-nt gap and a modified dCTP analog (orange). Residues Gly-274, Gly-290, and Arg-333 are highlighted in green in the structure. DNA is gray, and the enzyme is blue. Protein Data Bank (PDB) ID: 5UGP.

## 2. Materials and Methods

### 2.1. Protein Purification

A pET28-c plasmid encoding human WT Pol $\beta$  (as the *POLB* gene) or its variant G274R, G290C, or R333W (as *POLB* carrying an SNP) was transfected into *Escherichia coli* Rosetta 2 cells. Proteins' expression was induced by the addition of 0.1 mM isopropyl  $\beta$ -D-thiogalactopyranoside (IPTG) after optical density at 600 nm ( $OD_{600}$ ) reached 0.5–0.6 before harvesting of the cells via centrifugation. Cell pellets were resuspended in a buffer (20 mM HEPES-KOH, 40 mM NaCl, pH 7.8) and lysed via a French press. The lysate was centrifuged at  $40,000\times g$  for 40 min. For enzymes purification, two-stage chromatography on a Q-Sepharose column and Ni-NTA resin was performed. The collected protein fraction was dialyzed overnight against a buffer composed of, 20 mM HEPES-KOH pH 7.8, 150 mM NaCl and 20% glycerol. The pure protein fraction was supplemented with 50% glycerol and stored at  $-20\text{ }^{\circ}\text{C}$ . For more details, refer to [32].

### 2.2. DNA Substrates

Sequences of the oligodeoxyribonucleotides (containing a gap with 2'-deoxyribose phosphate) used in the work are given in Table 2. The 36-bp DNA substrates used in DNA-binding, strand displacement synthesis, and gap-filling assays were labeled with FAM at the 5' end of the primer strand and obtained by mixing equimolar amounts of three DNA strands: FAM\_Pol19, Pol\_36\_N, and Pol16. The DNA substrate subjected to the conformational dynamics analysis and containing a 2-aminopurine (2-aPu) residue was prepared by mixing equimolar amounts of Pol16, Pol19, and Pol36\_T\_Å. The DNA substrates were annealed for 5 min at  $93\text{ }^{\circ}\text{C}$  and allowed to cool down to room temperature.

**Table 2.** Sequences of oligodeoxyribonucleotides (containing a gap with 2'-deoxyribose phosphate) used in the work.

Name	Sequence
Pol16	5'-TAGTCACCTCAATCCA-3'
Pol19	5'-GCCTCGCAGCGGTCCAACC-3'
Pol19_FAM	FAM 5'-GCCTCGCAGCGGTCCAACC-3' *
Pol36_T_Å	5'-TGGATTGAGGTGACTÅNGGTTGGACGGCTGCGAGGC-3' *
Pol36_N:	5'-TGGATTGAGGTGACTANGGTTGGACGGCTGCGAGGC-3' *

\* where N = A/T/G/C, Å = 2-aPu residue, and FAM = 6-fluorescein residue.

### 2.3. Circular Dichroism Spectroscopy (CD)

CD spectra were recorded on a Jasco J-600 spectropolarimeter (Jasco, Tokyo, Japan). The enzyme solutions were prepared in a buffer composed of 50 mM Tris-HCl, pH 7.5, 50 mM KCl, 1.0 mM EDTA, and 5.0 mM MgCl<sub>2</sub>, and were placed in quartz cuvettes with a light path length of 0.1 mm. Spectra with a bandwidth of 1.0 nm and a wavelength ranging from 190 to 260 nm were acquired. Automatic averaging was done when the measurements were taken. An online tool for choosing and modeling protein CD spectra was used to describe the spectra [33–35].

### 2.4. Analysis of the Melting Point of the Enzymes

The 50 μM samples of enzymes were prepared in a buffer (50 mM Tris-HCl pH 7.5, 50 mM KCl, 1.0 mM EDTA, 5.0 mM MgCl<sub>2</sub>) and supplemented with 5× ProteOrange dye (Lumiprobe, Moscow, Russia). Melting points were measured by means of a Quant Studio 5 real-time PCR system (Applied Biosystems, Waltham, MA, USA) in PCR tubes using the thermal shift assay. The temperature was constantly raised in steps of 0.028 °C, from 25.1 to 99.9 °C. The fluorescence intensity of the ProteOrange dye was recorded via excitation at 470 nm and emission at 558 nm. Each melting point value was calculated using the Boltzmann sigmoid curve equation:

$$F = F_u + (F_b - F_u) / \{1 + \exp(T_m - x / \text{slope})\}, \quad (1)$$

where F is ProteOrange fluorescence emission, x is temperature, F<sub>u</sub> is baseline fluorescence at low temperature, F<sub>b</sub> is maximum fluorescence at high temperature, the slope describes the steepness of the curve, and T<sub>m</sub> is the melting point of the protein.

### 2.5. DNA-Binding Analysis

The DNA–Polβ complexes were separated in a non-denaturing 10% PAAG (the ratio of acrylamide to N,N'-methylenebisacrylamide was 75:1) at 4 °C. The DNA-binding reaction samples were prepared in a buffer composed of 50 mM Tris-HCl pH 7.5, 50 mM KCl, 1 mM Na<sub>2</sub>EDTA, 5 mM MgCl<sub>2</sub>, 1 mM DTT, and 7% glycerol. The recombinant enzymes were serially diluted; for the Polβ G274R polymorphic variant, the concentration range was from 86 nM to 11 μM; for the G290C variant, the concentration range was 0.16 to 20 μM; and for the R333W variant, the concentration range was 0.9 to 115 μM. The concentration of FAM-labeled substrate Gap\_N was 50 nM. To determine the dissociation constant, the resultant gel was visualized in a VersaDoc gel-documenting system (Bio-Rad Laboratories, Hercules, CA, USA). The results were processed using the Gel-Pro Analyzer 4 software (Media Cybernetics, Rockville, MD, USA). The dissociation constant K<sub>d</sub> for each enzyme–DNA complex was computed in the OriginPro 8 software via the equation:

$$\text{Formed complex (\%)} = F_u + (F_b - F_u) / \{1 + (K_d / [\text{Pol}\beta])^h\}, \quad (2)$$

where h is the Hill coefficient, F<sub>u</sub> is the correction for background illumination, and F<sub>b</sub> is the maximum intensity of the complex.

### 2.6. Analysis of Polβ Variants' Polymerase Activity

The DNA elongation assay was performed in a buffer consisting of 50 mM Tris-HCl pH = 7.5, 50 mM KCl, 1 mM Na<sub>2</sub>EDTA, 5 mM MgCl<sub>2</sub>, 1 mM DTT, and 7% glycerol at 37 °C. The 5 μL reaction samples contained 0.5 μM Gap\_T substrate, 5 μM dNTP mix, and 0.5 μM enzyme. The reaction time was 1 min, and the reaction was stopped by mixing with 5 μL of a stop solution (7.5 M urea, 25 mM EDTA, 0.1% oxylene cyanol, and 0.1% of bromophenol blue). The separation of the reaction products was performed by denaturing 20% PAAG.

To determine the gap-filling activity of the G290C variant, the reaction mixture containing 0.5 μM Gap\_N substrate, 5 μM complementary dNTP, and 0.5 μM enzyme was used. The reaction was stopped by mixing with 5 μL of a stop solution (7.5 M urea, 25 mM

EDTA, 0.1% xylene cyanol, and 0.1% bromophenol blue) after 20, 40, 60, 90, or 120 s. The prepared samples were applied to a denaturing 15% PAAG.

All resulting gels were visualized in the VersaDoc gel-documenting system (Bio-Rad Laboratories, Hercules, CA, USA). The data were processed using the Gel-Pro Analyzer 4 software (Media Cybernetics, Rockville, MD, USA) and the degree of substrate conversion was determined by means of the ratio of the peak areas of the product to the sum of the peak areas of the product and the peak of the initial substrate. A relevant characteristic of the polymerase activity of Pol $\beta$  is the observed rate constant of the reaction of incorporation of various dNTPs into a synthesized DNA strand,  $k_{\text{obs}}$ . The final calculation of the observed reaction rate constant was carried out in the OriginPro 8 software via plotting of the dependence of the product accumulation on reaction time. The obtained data were fitted to the equation:

$$[\text{Product}] = [\text{S}] \times \{1 - \exp(-k_{\text{obs}} \times t)\}, \quad (3)$$

where [S] is the initial concentration of the substrate,  $t$  is reaction time, and  $k_{\text{obs}}$  is the observed rate constant of the chemical reaction.

### 2.7. Registration of Conformational Changes in the DNA Substrate by the Stopped-Flow Method and Determination of Polymerization Reaction Rate Constant $k_{\text{pol}}$ and Observed Constant $K_{\text{d,app(dATP)}}$ for the G290C Variant

Conformational changes in the DNA substrate containing a gap and 2-aPu residue were recorded at a fluorescence excitation wavelength of 310 nm. Registration of conformational changes in the substrate DNA was carried out on an SX.20MV stopped-flow spectrophotometer (Applied Photophysics, Leatherhead, UK).

A comparison of the effects of variants G274R, G290C, and R333W on the conformational dynamics of DNA was carried out at 37 °C. The concentration of the enzymes was 1.0  $\mu\text{M}$ , Gap\_T $\bar{\text{A}}$  DNA substrate concentration was 0.5  $\mu\text{M}$ , and dATP concentration was 100  $\mu\text{M}$ .

To determine the influence of the substitution of the amino acid residue in variant G290C on the catalytic step and the step of enzyme binding to dATP (formation of a ternary complex), the experiment was conducted by varying the concentration of dATP. Concentrations of the enzyme and DNA substrate were 1.0 and 0.5  $\mu\text{M}$ , respectively; varying concentrations of dATP were 50, 100, 150, 200, and 400  $\mu\text{M}$ . The reaction was carried out at 37 °C.

To determine the polymerization reaction rate constant  $k_{\text{pol}}$  and observed constant  $K_{\text{d,app(dATP)}}$  of dissociation of dATP from the enzyme–DNA complex, the region of the fluorescence curves corresponding to the slow stage of the decrease in fluorescence intensity of 2-aPu was fitted to the following equation [36]:

$$F = F_0 + F_1 \times \exp(-k_{\text{obs}} \times t), \quad (4)$$

where  $F$  is the observed 2-aPu fluorescence intensity signal,  $F_0$  is background fluorescence,  $F_1$  is a fluorescence parameter, and  $k_{\text{obs}}$  is the observed rate constant. From the obtained values of the observed rate constants, a dependence on the concentration of dATP was constructed. The resulting dependence was fitted to Equation (4), which enabled us to obtain parameters  $k_{\text{pol}}$  and  $K_{\text{d,app(dATP)}}$ :

$$k_{\text{obs}} = k_{\text{pol}}[\text{dATP}] / (K_{\text{d,app(dATP)}} + [\text{dATP}]), \quad (5)$$

where  $k_{\text{obs}}$  is the observed rate constant of the reaction,  $k_{\text{pol}}$  is the rate constant of the polymerization reaction, and  $K_{\text{d,app(dATP)}}$  is the dissociation constant of the enzyme–DNA–dATP complex.

### 2.8. Determination of Polymerization Reaction Rate Constant $k_{pol}$ and Observed Constant $K_{d,app(dATP)}$ for Variants G274R and R333W

To determine the influence of substitutions of amino acid residues in variants G274R and R333W on the catalytic step and the step of enzyme binding to dATP (formation of a ternary complex), the assay of separation of the reaction product in 15% PAAG was used. The experiments were conducted by varying the concentration of dATP. Concentrations of the G274R and R333W variants and DNA substrate were 1.0 and 0.5  $\mu\text{M}$ , respectively. The varying concentrations of dATP were 25, 75, 100, 200, and 400  $\mu\text{M}$  for the G274R variant and 25, 50, 75, 150, 250, and 750  $\mu\text{M}$  for the R333W variant. The reaction was allowed to proceed at 37 °C. All resulting gels were visualized in the VersaDoc gel-documenting system (Bio-Rad Laboratories, Hercules, CA, USA). Observed rate constants  $k_{obs}$  were calculated by means of Equation (3). The polymerization reaction rate constant  $k_{pol}$  and observed constant  $K_{d,app(dATP)}$  of dissociation of dATP from the enzyme–DNA complex was calculated using Equation (5) from the resulting dependency of  $k_{obs}$  on dATP concentration.

### 2.9. Molecular Dynamic Simulations (MD)

Human Pol $\beta$  apoenzyme structure was modeled by means of a crystal structure of rat Pol $\beta$  [37]. Models of the Pol $\beta$ –DNA open binary complex and Pol $\beta$ –DNA–dNTP ternary closed complex were based on crystal structures of human Pol $\beta$  complexes [15,38]. The DNA was edited to match experimental sequences, and the protein and the DNA primer were parametrized with the AMBER 14SB-OL15 force field set [39–41]. Homology and unstructured-region modeling was performed using Modeller [42]. Protein protonation states were assigned by PDB2PQR server with PROPKA [43,44]. Simulations were run with the help of the GROMACS 2022 MD package. A simulation box was set up with TIP3P water and 50 mM KCl JC ions [45,46]. Octahedral dummy model treatment was chosen for active-site magnesium ions [47]. RESP charges for nucleoside triphosphates were assigned using R.E.D. Server via an established approach [48,49]. Force field parameters were converted with ACPYPE [50]. The cutoff of nonbonded interactions was set to 0.8 nm, and long-range electrostatic interactions were treated via the PME method [51]. Bonds of hydrogen atoms were constrained using LINCS [52]. Flat-bottom potential restraints were applied to hydrogen-bonded heavy atoms of terminal base pairs in the truncated DNA primers. Steepest descent energy minimization was followed by 1 ns NVT and NPT equilibrations with heavy atom restraints. Unrestrained MD simulations were run in triplicate for 0.5 and 2  $\mu\text{s}$  for the N-terminal fragment using a V-rescale thermostat and C-rescale barostat [53,54]. Resultant trajectories were processed with the integrated GROMACS toolset. PCA calculations were performed and plotted in NMWiz.

## 3. Results

### 3.1. Effects of the Substitutions on Protein Structure and Melting Temperature

To test the impact of the selected amino acid substitutions on protein structure, experiments were conducted to obtain circular dichroism (CD) spectra (Figure 2a). The spectra were fitted using the <https://bestsel.elte.hu/> resource (accessed on 16 February 2023). The shape of the spectra obtained for variants G274R, G290C, and R333W had little difference from the spectrum obtained for WT Pol $\beta$ . The calculated amount of  $\alpha$ -helices contained in WT Pol $\beta$  was almost two times greater than that in the studied variants of the enzyme (Table 2), possibly indicating greater mobility of variants G274R, G290C, and R333W.

To clarify the effects of the substitutions on the physical properties of Pol $\beta$ , the melting temperature of the variants was measured by the thermal shift method. The enzyme samples were mixed with the intercalating dye ProteOrange and heated from 25.1 to 99.9 °C. The melting curves of WT Pol $\beta$  and its variants had similar shapes (Figure 2b). The melting temperature of variants G274R, G290C, and R333W, as calculated via fitting of the melting curves to Equation (1), was slightly lower than that of WT Pol $\beta$  (Table 3). Previously, for mutants of Pol $\beta$  containing various substitutions of amino acid residues, it

has been reported that such substitutions also do not lead to changes in the overall structure of the enzyme.

**Table 3.** Calculated contents of  $\alpha$ -helices and calculated melting points of the Pol $\beta$  variants.

	WT	G274R	G290C	R333W
$\alpha$ -helices, %	79 $\pm$ 16 *	48 $\pm$ 10	33 $\pm$ 7	34 $\pm$ 7
$T_m$ , °C	44.9 $\pm$ 0.2 **	42 $\pm$ 1	42.5 $\pm$ 0.9	41 $\pm$ 1

\* from Ref. [32]; \*\* from Ref. [55].

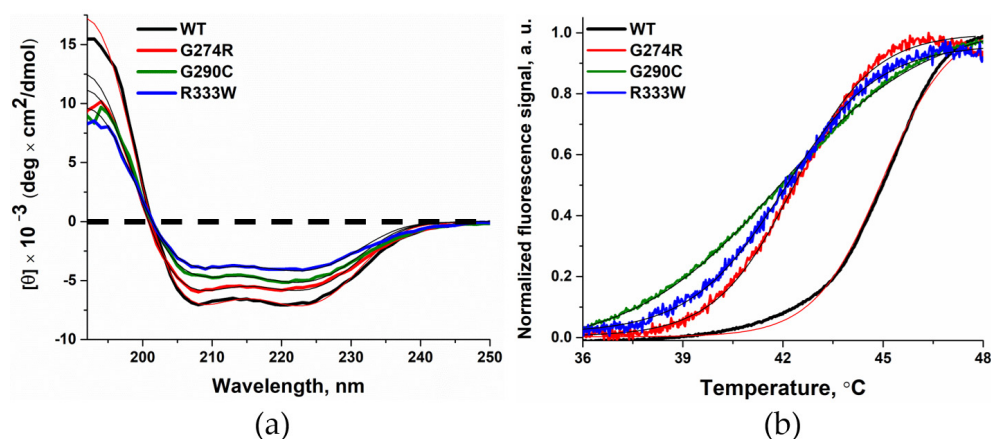


**Figure 2.** The influence of substitutions G274R (red), G290C (green), and R333W (blue) on Pol $\beta$  secondary structure (a) and thermal stability (b). Data on WT Pol $\beta$ , G274R, G290C, R333W are shown in black, red, green and blue respectively. Fitted lines for G274R, G290C, and R333W are indicated as thin black lines; fitted lines for WT Pol $\beta$  are indicated as thin red lines.

For more detailed analysis, molecular dynamics (MD) simulations of the Pol $\beta$  apoenzyme and of the polymorphic variants were performed next. Pol $\beta$  is a protein of which considerable conformational mobility in the apoenzyme has been documented. The variants in question—G274R, G290C, and R333W—were found to have similar mobility in the MD simulations, and no considerable differences from WT Pol $\beta$  were detectable (Figure 3a).

Examination of the MD simulation data on the immediate environment of the analyzed amino acid residues showed that the G290C polymorphic variant is the least different from the WT in this regard (Figure 3c). The WT Pol $\beta$  apoenzyme and variant G290C retain a more open conformation. Cys-290 does not engage in any new contacts in contrast to WT Pol $\beta$ .

For the G274R variant, it was revealed that the side chain of Arg-274 is mobile and can form hydrogen bonds and salt bridges with many catalytically important amino acid residues (Figure 3b) such as Asp-190, Asp-192, and Asp-256, coordinating the magnesium ion necessary for the transferase reaction.

Two stable structures were obtained for the R333W polymorphic variant. In the first one, which existed most of the time (Figure 3d, yellow), the introduction of the larger residue (Trp-333) caused a restructuring of the network of hydrogen bonding contacts. In this case, residue Trp-333 is in a stacking interaction with Pro-320 and Phe-278. The overall structure of the dNTP selection subdomain is preserved. The second possible consequence of the introduction of the R333W substitution may be the unfolding of the C-terminal region (Figure 3d, gray). Such protein folding may affect the activity of the enzyme.

Thus, the obtained data, together with the results of the thermal shift assay and analysis of the CD spectra, suggested that the introduction of substitution G274R, G290C, or R333W into Pol $\beta$  does not lead to considerable structural changes, at least in the apoenzyme. Nonetheless, the G274R and R333W substitutions changed the natural local network of contacts near the respective amino acid residues, which may affect further enzymatic stages.

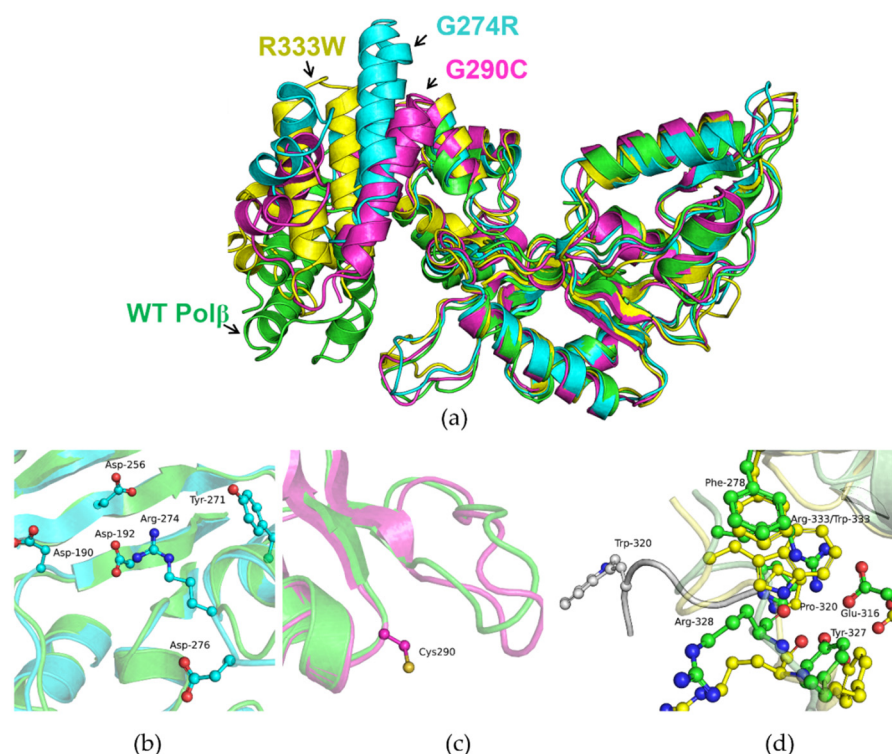


**Figure 3.** (a) An overlay of apoenzyme structures of WT Pol $\beta$  and variants G274R, G290C, and R333W as a result of MD simulations. WT Pol $\beta$ : green, G274R: blue, G290C: magenta, R333W: yellow. Close-ups of the microenvironment of amino acid residues Arg-274 (b), Cys-290 (c), Trp-333 (d). The variants of Pol $\beta$  manifested similar MD and little difference from the WT enzyme.

### 3.2. Determining the Effect on the Formation of the Complex with DNA

To determine the effect of these amino acid substitutions on the stage of formation the binary complex with DNA, the electrophoretic mobility shift assay in a non-denaturing gel was used. DNA substrates contained a 1-nt gap with a different nucleotide placed in the opposite strand (Gap\_A, Gap\_T, Gap\_G, and Gap\_C) and were FAM-labeled on the elongated strand. The different complementary DNA strands, which allowed the placement of different nucleotides opposite the 1-nt gap, were employed to check the influence of various bases on the efficiency of binary enzyme–DNA complex formation. The structure of the DNA substrate is presented in Figure 4 and in the Materials and Methods section. For variants G274R, G290C, and R333W, several complexes (with DNA) having different mobility were detectable. The formation of such DNA complexes is also characteristic of WT Pol $\beta$  [56].

To characterize the impact of the substitutions G274R, G290C, and R333W on the efficiency of DNA-binding, the percentage ratio of free DNA to DNA in complex with the enzyme was calculated. From the dependence of the obtained ratio on the change in enzyme concentration in the reaction, the dissociation constant of the Pol $\beta$ –DNA complex was calculated using Equation (2) (Figure 5). All the tested polymorphic variants had a weaker affinity for DNA than the WT enzyme did (Table 4). The obtained dissociation constant  $K_d$  values differed when DNA substrates containing different nucleotides opposite the 1-nt gap were analyzed. The effects on the formation of the complex with DNA were similar between substitutions G274R and G290C; a weakening of the affinity of the enzymes for DNA by approximately 3–4-fold was recorded on average. The largest increase in  $K_d$  was obtained for the R333W variant: by 10-fold on average, depending on the type of nucleotide located opposite the 1-nt gap in the DNA substrate.

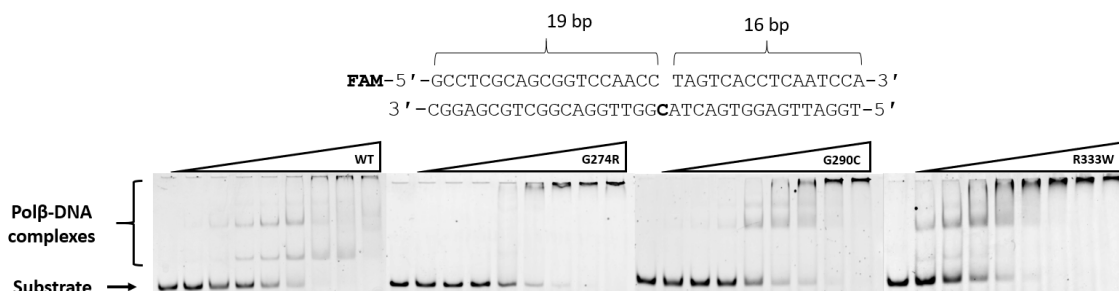


**Figure 4.** DNA-binding efficiency of WT Pol $\beta$  and of polymorphic variants G274R, G290C, and R333W toward substrate Gap\_C. Compared to the WT, the Pol $\beta$  variants showed less effective complex formation with this DNA substrate. For the G274R variant, a clear-cut band related to the complex of the enzyme with DNA was less intense than for variants G290C and R333W. WT Pol $\beta$  concentration: 22 nM to 2.63  $\mu$ M, G274R concentration: 86 nM to 11  $\mu$ M, G290C concentration: 0.16  $\mu$ M to 20  $\mu$ M, R333W concentration: 0.9  $\mu$ M to 115  $\mu$ M. The concentration of FAM-labeled DNA was 50 nM. Original figures can be found in Supplementary Materials.

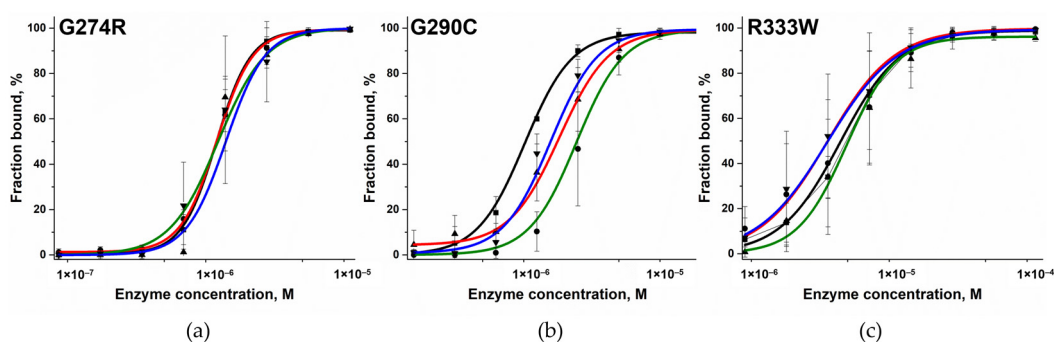


**Figure 5.** Complex formation efficiency of polymorphic variants G274R (a), G290C (b), and R333W (c) toward DNA substrates containing different nucleotides opposite the 1-nt gap [black: Gap\_A (■), red: Gap\_T (●), green: Gap\_G (▲), and blue: Gap\_C (▼)]. G274R concentration: 86 nM to 11  $\mu$ M, G290C concentration: 0.16  $\mu$ M to 20  $\mu$ M, R333W concentration: 0.9  $\mu$ M to 115  $\mu$ M. The concentration of FAM-labeled DNA was 50 nM.

**Table 4.** Calculated dissociation constants  $K_d$  ( $\mu$ M) of the complexes of variant G274R, G290C, and R333W with DNA.

	Gap_A	Gap_T	Gap_G	Gap_C
WT *	0.38 $\pm$ 0.02	0.33 $\pm$ 0.03	0.59 $\pm$ 0.07	0.38 $\pm$ 0.03
G274R	1.10 $\pm$ 0.09	1.4 $\pm$ 0.1	1.2 $\pm$ 0.1	1.4 $\pm$ 0.1
G290C	1.0 $\pm$ 0.1	1.8 $\pm$ 0.1	2.4 $\pm$ 0.2	1.6 $\pm$ 0.1
R333W	4.4 $\pm$ 0.2	3.6 $\pm$ 0.4	4.9 $\pm$ 0.6	3.6 $\pm$ 0.2

\* from Ref. [32].

For a more detailed understanding of possible rearrangements near the replaced amino acid residues during the formation of a complex with DNA, MD simulations of complexes of the Pol $\beta$  variants with DNA were carried out next (Figure 6).

During the MD simulation analysis, it was revealed that the Arg-274 residue can form contact with the phosphate group of the nucleotide located opposite the gap and with the O5' atom of the downstream nucleotide (Figure 6a).

In MD simulations of the complex of variant G290C with DNA, the changes introduced by the mutation were poorly distinguishable from the general background because the complexes have substantial mobility. The C-terminal region of the G290C polymorphic

variant proved to be more mobile than that of WT Pol $\beta$ . It was noted that the introduction of the cysteine residue at position 290 induces a redistribution of contacts in the binary complex: the amide group of Asn-279 forms hydrogen bonds with the backbone oxygen atom of Ser-275, while in the WT, bonds involving O(Leu-270) and O(Tyr-271) are more dominant (Figure 6b).

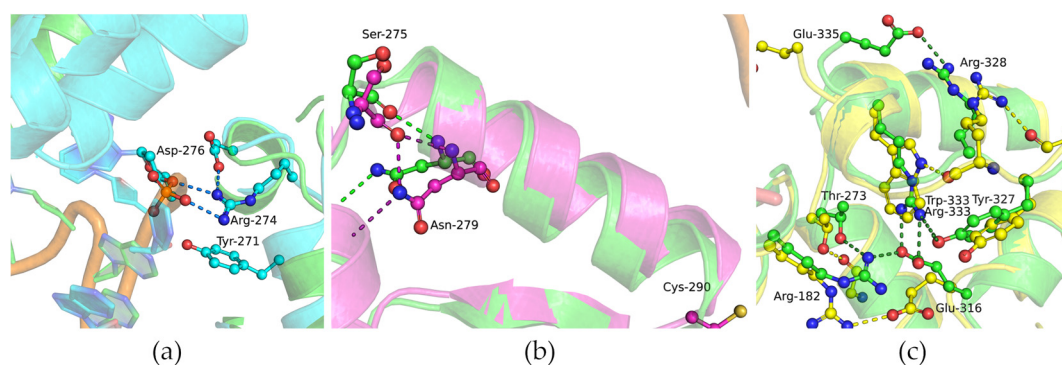


**Figure 6.** Overlays of snapshots of the dNTP selection subdomain in an open binary protein–DNA complex. The overlay of WT Pol $\beta$  (green) and G274R (cyan) (a). The overlay of WT Pol $\beta$  (green) and G290C (magenta) (b). The overlay of WT Pol $\beta$  (green) and R333W (yellow) (c). Salt bridges between amino acid side chains and the sugar-phosphate backbone are shown as dashed lines.

An even more pronounced redistribution of contacts occurred when Arg-333 was replaced by Trp (Figure 6c). This substitution impaired DNA-binding and increased the dissociation constant of the binary complex.

Taken together, these findings indicate an influence of substitutions G274R, G290C, and R333W on the stage of binding to the DNA substrate. Substitutions G274R and G290C led to a slight increase in the dissociation constant  $K_d$  and a slight redistribution of contacts near DNA-binding sites. In this context, variant R333W manifested the greatest difference from WT Pol $\beta$ ; the replacement of the R333 residue elevated  $K_d$  by 10-fold and induced a greater redistribution of contacts formed by Arg-333 in WT Pol $\beta$ .

### 3.3. Determination of the Gap-Filling Efficiency of the Pol $\beta$ Variants

Many known amino acid substitutions generated by SNPs weaken polymerase activity of Pol $\beta$  during the filling of a 1-nt gap and during extension of the primer strand [27,32,55,57]. To investigate the influence of amino acid substitutions G274R, G290C, and R333W on the polymerase activity of the enzyme, products of the enzymatic reaction were separated by polyacrylamide gel (PAAG) electrophoresis. The reaction was carried out by mixing a solution of a FAM-labeled DNA substrate containing a 1-nt gap, a complementary dNTP, and the enzyme. In the assay of the ability of the Pol $\beta$  variants to elongate the DNA strand containing the 1-nt gap, it was shown that only the G290C variant can extend a DNA strand, whereas the attachment of new nucleotides occurred more slowly as compared to the WT enzyme (Figure 7a). For variants G274R and R333W under the chosen conditions (0.5  $\mu$ M DNA, 0.5  $\mu$ M enzyme, and 5  $\mu$ M dNTP), the accumulation of the reaction product was undetectable, indicating a considerable degree of enzyme inactivation.

To evaluate the only ability of the G290C variant (gap-filling), an experiment was conducted in the presence of various triphosphates by means of four types of DNA substrates containing different nucleotides opposite the 1-nt gap (Figure 7b). Observed reaction rate constants  $k_{obs}$  were calculated using Equation (3) and were, on average, three times lower relative to WT Pol $\beta$  (Table 5). Similarly to WT Pol $\beta$ , the incorporation of dCMP by the variants into the 1-nt gap was the least efficient.

**Table 5.** Observed reaction rate constants  $k_{\text{obs}}$  for the incorporation of a complementary nucleotide into the tested DNA substrates containing a 1-nt gap.

	Gap_A	Gap_T	Gap_G	Gap_C
WT *	$0.33 \pm 0.03$	$0.32 \pm 0.04$	$0.25 \pm 0.02$	$0.34 \pm 0.02$
G290C	$0.12 \pm 0.02$	$0.081 \pm 0.002$	$0.063 \pm 0.003$	$0.10 \pm 0.02$

\* from Ref. [32].

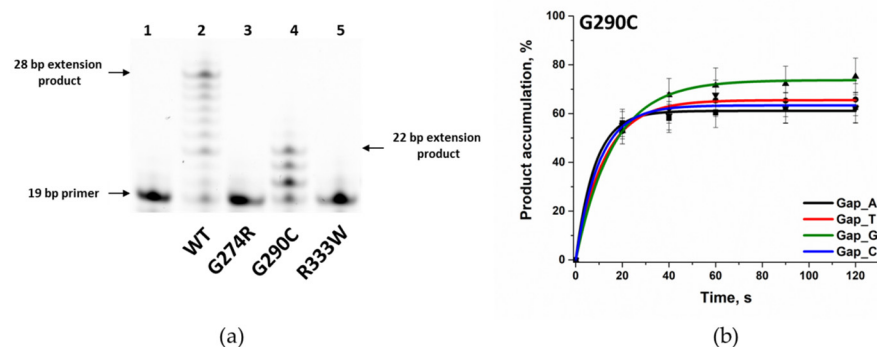


**Figure 7.** (a) A comparison of the effectiveness of strand replacement synthesis by Pol $\beta$  variants G274R, G290C, and R333W. In lane 1 is 19-Nucleotide FAM-labeled DNA primer Gap\_T, primer extension by WT Pol $\beta$  is presented in lane 2, primer extension by the G274R variant is in lane 3, primer extension by the G290C variant is in lane 4, and primer extension by the R333W variant is in lane 5. WT Pol $\beta$  generated products up to 30 nt in length within 1 min of the reaction by elongating the DNA primer by up to 11 nt. Variant G290C proved to be a less active polymerase compared to WT Pol $\beta$ . The G290C variant extended the primer by 3 nt. Variants G274R and R333W did not elongate the DNA within the given reaction timeframe. The dNTP mix concentration was 10  $\mu\text{M}$ , the enzymes' and DNA concentrations were 0.5  $\mu\text{M}$ , and the temperature was 37  $^{\circ}\text{C}$ . The reaction time was 1 min. (b) Single-nucleotide incorporation by the G290C variant. The dNTP concentration was 5  $\mu\text{M}$ , the enzyme and DNA concentrations were 0.5  $\mu\text{M}$ , and the temperature was 37  $^{\circ}\text{C}$ .

### 3.4. dNTP Binding and Incorporation

The detected change in the polymerase activity of the Pol $\beta$  variants G274R, G290C, and R333W may be explained not only by the shift of affinity for 1-nt gap-containing DNA but also by a change in the ability to bind complementary dNTPs. For many polymorphic variants of Pol $\beta$ , there is evidence of a decrease in observed dissociation constant  $K_{\text{d,app}}(\text{dATP})$ , as well as a decrease in polymerization constant  $k_{\text{pol}}$  (reflecting the rate of the chemical stage) [32,55].

It is known that when interacting with DNA and triphosphates, Pol $\beta$  undergoes several stages of conformational alterations [36]. In this case, the changes in conformation occur not only in the enzyme but also in the DNA: it bends by  $\sim 90^{\circ}$  [58]. To record such conformational changes, the stopped-flow method was used with a DNA substrate containing a 1-nt gap and a fluorescent base analog: 2-aminopurine (2-aPu). When the environment changes from hydrophobic to hydrophilic, a 2-aPu residue can change its fluorescence intensity [59–61]. To determine the binding parameters of variants G274R, G290C, and R333W here, various concentrations of complementary triphosphate were added to the reaction.

The interaction of two almost inactive variants (G274R and R333W) with the DNA substrate did not alter the fluorescence intensity of the 2-aPu residue incorporated into the DNA (Figure 8a). The Trp residue has its own fluorescence too; conformational dynamics of many enzymes can be recorded when tryptophan residues are present in the protein globule [62]. WT Pol $\beta$  contains one Trp (at position 325), whose change in intensity is insufficient to register the conformational dynamics of the enzyme. The introduction of an additional Trp (at position 333) into the protein globule also did not allow for the detection of changes in the fluorescence intensity of Trp residues.

The active variant G290C caused changes in the fluorescence intensity of the 2-aPu residue when interacting with the DNA substrate. The determined changes differed from those reported in the literature for WT Pol $\beta$  (Figure 8a,b). The amplitude of the signal was lower compared with WT Pol $\beta$ , whereas the phase of decline of 2-aPu fluorescence intensity observed after 0.2 s was within the same timeframe in comparison with WT Pol $\beta$ . Earlier, it has been demonstrated that the decrease phase of fluorescence intensity of 2-aPu corresponds to the stage of accumulation of the reaction product [36]. To determine the binding parameters of polymorphic variant G290C toward dATP and to measure the polymerization constant, the part of the curve matching the decrease in fluorescence intensity of 2-aPu was fitted to Equation (4). By means of the obtained values of the observed reaction rates, a dependence on the concentration of dATP in the reaction was plotted and then calculated using Equation (5) (Figure 8c). The calculated value of  $k_{\text{pol}}$  was 1.3 times higher than that for WT Pol $\beta$  (Table 6). It is possible that the introduction of the G290C substitution does not affect the catalytic stage. On the other hand,  $K_{\text{d,app(dATP)}}$  was almost 4 times higher as compared to WT Pol $\beta$ . It can be concluded that the overall decrease in the polymerase activity of the G290C variant is related to effects on the stage of binding to dNTP, as well as to the weaker affinity for DNA shown above, but not to the impact of the substitution on catalysis.

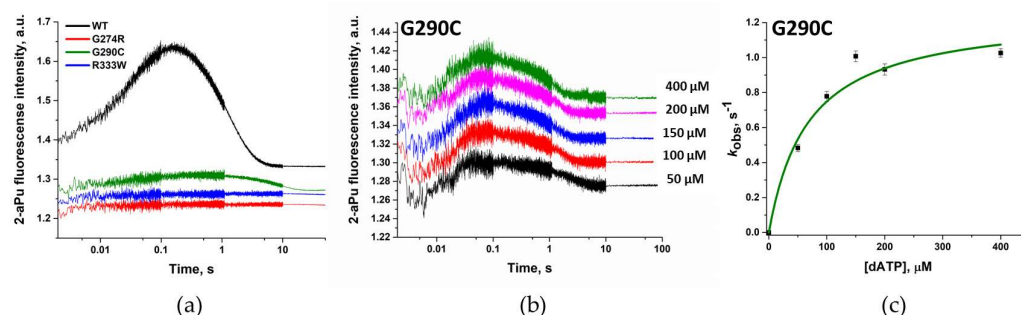


**Figure 8.** (a) A comparison of changes in the fluorescence intensity of a 2-aPu residue, which is part of a DNA substrate, during interaction with WT Pol $\beta$  or variant G274R, G290C, or R333W. [Enzyme] = 1.0  $\mu\text{M}$ , [Gap\_T $\ddot{\text{A}}$ ] = 0.5  $\mu\text{M}$ , [dATP] = 100  $\mu\text{M}$ . (b) Changes in the fluorescence intensity of a 2-aPu residue incorporated into DNA during interaction with the G290C variant at various dATP concentrations. [Enzyme] = 1.0  $\mu\text{M}$ , [Gap\_T $\ddot{\text{A}}$ ] = 0.5  $\mu\text{M}$ . (c) The dependence of calculated values of the observed reaction rate constants on the dATP for the polymorphic variant G290C.

For Pol $\beta$  variants G274R and R333W, for which it was impossible to register changes in 2-aPu fluorescence intensity, observed rate constant  $k_{\text{pol}}$  and  $K_{\text{d,app(dATP)}}$  were determined by detecting the accumulation of the polymerase reaction product with the help of PAAG electrophoresis at high concentrations of complementary dATP and a longer time scale. With an increase in these parameters, it was possible to register the accumulation of the reaction product (Figure 9a). The  $k_{\text{pol}}$  and  $K_{\text{d,app(dATP)}}$  values were determined by plotting the dependences of the observed reaction rate constant (calculated via Equation (3)) on the concentration of triphosphates in the reaction (Figure 9b,c). The resulting dependence was approximated as Equation (5) (Figure 10a,b).

For both variants G274R and R333W, an increase in  $k_{\text{pol}}$  and  $K_{\text{d,app(dATP)}}$  was observed (Table 6). Pol $\beta$  variants G274R and R333W showed an approximately 20-fold weakening of dATP-binding affinity and a 50-fold decrease in polymerization efficiency; these data reflect the influence of these amino acid substitutions on all the analyzed stages of the interaction of Pol $\beta$  with the substrates. For previously studied Pol $\beta$  variants at position 333, a high degree of enzyme inactivation has been documented too, varying with the type of substituted amino acid residue [29].

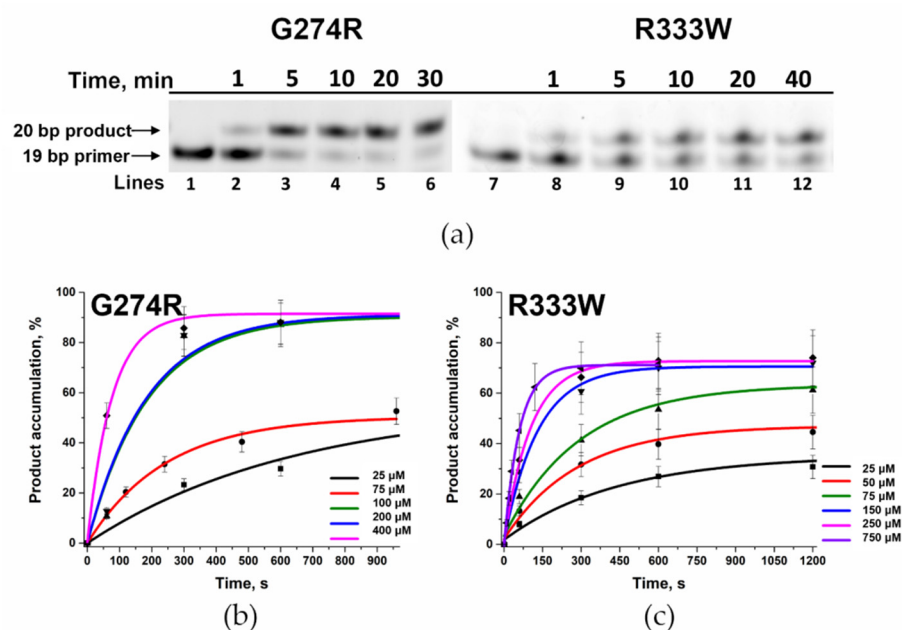


**Figure 9.** (a) Accumulation of the product of the gap-filling reaction performed on substrate Gap\_T DNA by polymorphic variants G274R and R333W. The enzyme concentration was 0.5 μM, DNA concentration was 0.5 μM, and dATP concentration was 100 and 75 μM for G274R and R333W, respectively. Lanes 1 and 7 contain the FAM-labeled Gap\_T substrate, lanes 2, 3, 4, 5, and 6 correspond to time points of 1, 5, 10, 20, or 30 min of the reaction with the Polβ G274R variant. Lanes 8, 9, 10, 11, and 12 represent time points of 1, 5, 10, 20, and 40 min of the reaction with variant R333W. The dependence of the product accumulation on time at various concentrations of dATP in the reaction is depicted in panels (b,c) for polymorphic variants G274R and R333W, respectively.

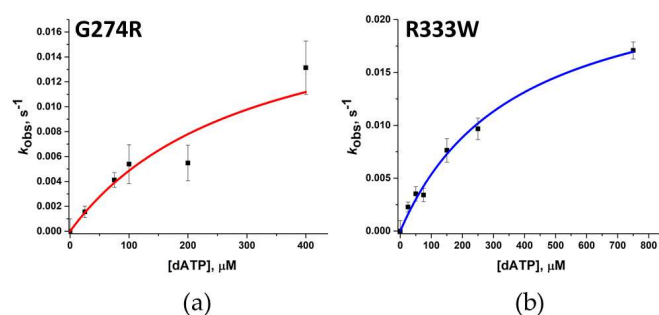


**Figure 10.** The dependence of calculated values of the observed reaction rate constants on the dATP concentration is displayed in panels (a,b) for the polymorphic variants G274R and R333W, respectively.

**Table 6.** Chemical reaction rate constants  $k_{pol}$  and observed dissociation constants  $K_{d,app(dATP)}$ .

	$k_{pol}, s^{-1}$	$K_{d,app(dATP)}, \mu M$
WT *	$0.93 \pm 0.05$	$16 \pm 3$
G274R	$0.019 \pm 0.008$	$306 \pm 168$
G290C	$1.2 \pm 0.1$	$62 \pm 21$
R333W	$0.025 \pm 0.002$	$374 \pm 75$

\* from Ref. [32].

For a more detailed consideration of the effect of substitutions G274R, G290C, and R333W on the dNTP-binding stage of the catalytic reaction, MD simulations of the complex of the enzyme with DNA and dNTP (ternary closed complex) were carried out.

Replacing Gly-274 with Arg led to the possible conformations involving a change in the coordination of the 3' oxygen atom of the primer nucleotide: this atom became coordinated with Arg-258 (Figure 11a). This conformation made it impossible to attach a new nucleotide monophosphate. Incorrect coordination of the primer nucleotide resulted in a decrease in the polymerization constant of the G274R variant by almost 50-fold, as compared to WT Pol $\beta$ .

In MD simulations of the G290C variant, the location and positioning of the Cys-290 residue remained the same as in WT Pol $\beta$ . Nevertheless, the alterations affected the flexible loop (aa 203–209) (Figure 11b). In WT Pol $\beta$ , Pro-208 is predominantly located at the beginning of the  $\alpha$ -helix and can form the N(Pro-208)–O(His-212) hydrogen bond. In the polymorphic variant, Pro-208 is mostly turned toward the loop. Besides, a redistribution of Thr-233 contacts was noted. In WT Pol $\beta$ , Thr-233 interacts with a DNA phosphate group, the backbone oxygen atom of Leu-268, and the side chain of Arg-258. In the G290C polymorphic variant, Thr-233 is turned predominantly toward the solution or DNA.

The MD simulations of the R333W variant's micro positioning in the ternary closed complex did not reveal appreciable differences from WT Pol $\beta$  (Figure 11c). Nonetheless, it has been previously shown that replacing Arg-333 with other amino acid residues causes a loss of contacts necessary for the normal functioning of Pol $\beta$  [29]. According to MD simulations of the R333E mutant, Glu-333 moves away from the site that was previously occupied by Arg-333 in the WT structure. The relocation of Glu-333 leads to a considerable rearrangement of the main chain and side chain positioning of residues Tyr-327, Arg-328, and Glu-329. It was shown that the intact triadic interaction between Arg-182, Glu-316, and Arg-333 is required for proper polymerase function.

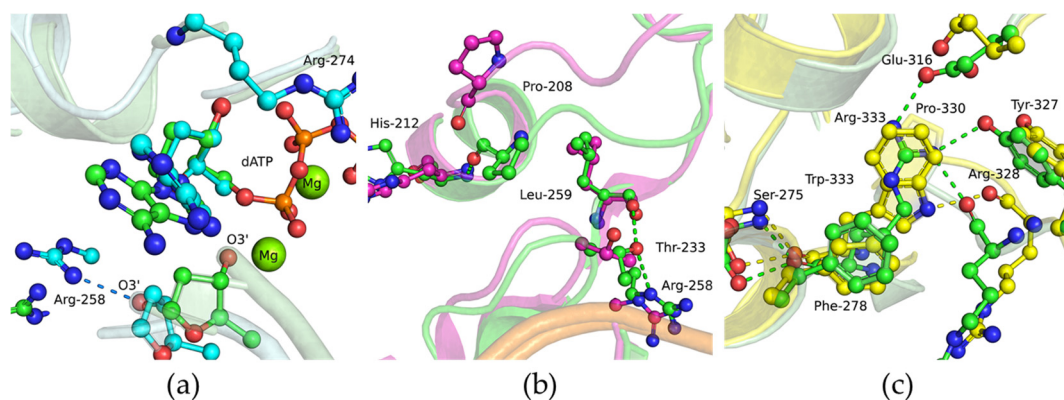


**Figure 11.** Snapshots of the micro arrangement of the protein–DNA–dNTP ternary complex involving variant G274R (a), G290C (b), or R333W (c) compared with WT Pol $\beta$ . Salt bridges between amino acid side chains and the sugar–phosphate backbone are presented as dashed lines. WT Pol $\beta$ : green, G274R: cyan, G290C: magenta, and R333W: yellow.

#### 4. Conclusions

DNA polymerase  $\beta$  is an enzyme that take part in many processes in the cell that are aimed at preserving genetic information. Today, many mutants of the enzyme are known to occur in various types of tumors. Some of these variants are caused by SNP-induced amino acid substitutions. Several of these amino acid substitutions in Pol $\beta$  may not have a considerable effect on the functioning of the enzyme; however, many Pol $\beta$  mutations are known that lead to a decrease in polymerase activity and in the fidelity of the addition of a complementary nucleotide. In this work, Pol $\beta$  polymorphic variants G274R, G290C, and R333W were characterized, which feature amino acid substitutions located in the dNTP selection subdomain (responsible for the correct addition of a complementary

dNMP). By CD spectroscopy, it was shown that these amino acid substitutions do not induce considerable alterations in the protein globule, and measurement of the melting temperature point of the enzymes did not reveal valuable differences from WT Pol $\beta$ . Using molecular dynamics methods, it was shown that substitutions G274R and R333W lead to a greater extent to the redistribution of local contacts during the interaction of the enzyme with DNA. In contrast, in G290C, amino acid substitution did not lead to a major change in local contacts with DNA. Experimental testing of the ability of the Pol $\beta$  variants G274R, G290C, and R333W to bind DNA containing a 1-nt gap detected a slight decrease in DNA-binding constants. Moreover, the  $K_d$  values for the G290C and R333W variants were higher than for the G274R variant. However, the  $K_d$  values for all three variants were higher than for the WT Pol $\beta$ , which is in agreement with the MD analysis of the redistribution of local contacts.

Kinetic analysis of enzymatic properties of the Pol $\beta$  variants uncovered a greater degree of inactivation in variants G274R and R333W compared to WT Pol $\beta$ . MD analysis revealed no possible conformations in which the G274R variant can support the transferase reaction. The data obtained for the R333W variant suggested the importance of Arg-333 for Pol $\beta$  functioning. Variant G290C was active but turned out to be a slower polymerase than WT Pol $\beta$ , owing to a weaker affinity for DNA, as well as an increase in observed binding constant  $K_{d, app}$  (dATP). An MD simulation revealed differences in the microenvironment of the substituted amino acid residues; these alterations may be a reason for the lowered activity of the Pol $\beta$  variants under study.

In general, our examination of the enzymatic properties of the natural polymorphic variants of Pol $\beta$  G274R, G290C, and R333W allows us to outline the influence of these amino acid substitutions on enzyme activity. For all variants, a decrease in polymerase activity was shown due to the redistribution of local contacts. The observed decrease in enzymatic activity may lead to a higher number of unrepaired DNA damage sites, which in turn leads to an increase in the number of mutations in the genome and thus can lead to malignant transformation of the cell.

**Supplementary Materials:** The following supporting information can be downloaded at: <https://www.mdpi.com/article/10.3390/biom14050547/s1>, Original Western Blots images.

**Author Contributions:** N.A.K., O.A.K., A.A.K. and T.E.T. conceived and designed the experiments; O.A.K. and A.A.M. conducted the experiments; O.A.K., A.A.M., N.A.K., A.A.K. and T.E.T. analyzed the data; D.S.N. performed the oligodeoxyribonucleotide synthesis, T.E.T. performed the MD simulation analysis. All authors have read and agreed to the published version of the manuscript.

**Funding:** The part of the work involving mutagenesis, enzyme purification, and kinetic analysis was specifically funded by the Russian Science Foundation, grant No. 21-74-10103. Partial governmental support for equipment use was received from the Russian Ministry of Science and Higher Education project No. 121031300041-4.

**Institutional Review Board Statement:** Not applicable.

**Informed Consent Statement:** Not applicable.

**Data Availability Statement:** Raw experimental data are available from O.A.K. and A.A.K. upon request. Tel. +7 (383) 363-5174, E-mail: kladova@niboch.nsc.ru (O.A.K.); sandra-k@niboch.nsc.ru (A.A.K.).

**Acknowledgments:** Computational resources were provided by the Computational Center of Novosibirsk State University.

**Conflicts of Interest:** The authors declare no conflicts of interest.

## References

1. Lindahl, T. Instability and Decay of the Primary Structure of DNA. *Nature* **1993**, *362*, 709–715. [[CrossRef](#)] [[PubMed](#)]
2. Retèl, J.; Hoebee, B.; Braun, J.E.; Lutgerink, J.T.; van den Akker, E.; Wanamarta, A.H.; Joenje, H.; Lafleur, M.V. Mutational Specificity of Oxidative DNA Damage. *Mutat. Res.* **1993**, *299*, 165–182. [[CrossRef](#)] [[PubMed](#)]
3. Marnett, L.J. Oxy Radicals, Lipid Peroxidation and DNA Damage. *Toxicology* **2002**, *181–182*, 219–222. [[CrossRef](#)]

4. Whitaker, A.M.; Schaich, M.A.; Smith, M.S.; Flynn, T.S.; Freudenthal, B.D. Base Excision Repair of Oxidative DNA Damage: From Mechanism to Disease. *Front. Biosci.—Landmark* **2017**, *22*, 1493–1522. [[CrossRef](#)] [[PubMed](#)]
5. Lomax, M.E.; Folkes, L.K.; O’Neill, P. Biological Consequences of Radiation-Induced DNA Damage: Relevance to Radiotherapy. *Clin. Oncol.* **2013**, *25*, 578–585. [[CrossRef](#)] [[PubMed](#)]
6. Hsieh, P. Molecular Mechanisms of DNA Mismatch Repair. *Mutat. Res.* **2001**, *486*, 71–87. [[CrossRef](#)] [[PubMed](#)]
7. Krokan, H.E.; Bjørås, M. Base Excision Repair. *Cold Spring Harb. Perspect. Biol.* **2013**, *5*, a012583. [[CrossRef](#)]
8. Fromme, J.C.; Verdine, G.L. Base Excision Repair. In *Advances in Protein Chemistry*; Academic Press: Cambridge, MA, USA, 2004; Volume 69, pp. 1–41.
9. Ide, H.; Kotera, M. Human DNA Glycosylases Involved in the Repair of Oxidatively Damaged DNA. *Biol. Pharm. Bull.* **2004**, *27*, 480–485. [[CrossRef](#)] [[PubMed](#)]
10. Jacobs, A.L.; Schär, P. DNA Glycosylases: In DNA Repair and Beyond. *Chromosoma* **2012**, *121*, 1–20. [[CrossRef](#)] [[PubMed](#)]
11. Liu, P.; Burdzy, A.; Sowers, L.C. Substrate Recognition by a Family of Uracil-DNA Glycosylases: UNG, MUG, and TDG. *Chem. Res. Toxicol.* **2002**, *15*, 1001–1009. [[CrossRef](#)]
12. Tell, G.; Quadrioglio, F.; Tiribelli, C.; Kelley, M.R. The Many Functions of APE1/Ref-1: Not Only a DNA Repair Enzyme. *Antioxid. Redox Signal* **2009**, *11*, 601–619. [[CrossRef](#)]
13. Fung, H.; Demple, B. A Vital Role for Ape1/Ref1 Protein in Repairing Spontaneous DNA Damage in Human Cells. *Mol. Cell* **2005**, *17*, 463–470. [[CrossRef](#)] [[PubMed](#)]
14. Sobol, R.W.; Wilson, S.H. Mammalian DNA Beta-Polymerase in Base Excision Repair of Alkylation Damage. *Prog. Nucleic Acid Res. Mol. Biol.* **2001**, *68*, 57–74. [[PubMed](#)]
15. Sawaya, M.R.; Prasad, R.; Wilson, S.H.; Kraut, J.; Pelletier, H. Crystal Structures of Human DNA Polymerase Beta Complexed with Gapped and Nicked DNA: Evidence for an Induced Fit Mechanism. *Biochemistry* **1997**, *36*, 11205–11215. [[CrossRef](#)] [[PubMed](#)]
16. Dianov, G.L.; Prasad, R.; Wilson, S.H.; Bohr, V.A. Role of DNA Polymerase  $\beta$  in the Excision Step of Long Patch Mammalian Base Excision Repair. *J. Biol. Chem.* **1999**, *274*, 13741–13743. [[CrossRef](#)] [[PubMed](#)]
17. Prasad, R.; Lavrik, O.I.; Kim, S.-J.; Kedar, P.; Yang, X.-P.; Vande Berg, B.J.; Wilson, S.H. DNA Polymerase  $\beta$ -Mediated Long Patch Base Excision Repair. Available online: <https://reader.elsevier.com/reader/sd/pii/S0021925820777550?token=AB86DB76EB9167C69BF33CC20A6473F65E81FDCB8BC20B7DF2D8C1DE8FD345E4A99A08EA7CDDAB5B6FD6F55CB7B5A220&originRegion=eu-west-1&originCreation=20210618070314> (accessed on 18 June 2021).
18. Kumar, A.; Widen, S.G.; Williams, K.R.; Kedar, P.; Karpel, R.L.; Wilson, S.H. Studies of the Domain Structure of Mammalian DNA Polymerase Beta. Identification of a Discrete Template Binding Domain. *J. Biol. Chem.* **1990**, *265*, 2124–2131. [[CrossRef](#)] [[PubMed](#)]
19. Menge, K.L.; Hostomsky, Z.; Nodes, B.R.; Hudson, G.O.; Rahmati, S.; Moomaw, E.W.; Almasy, R.J.; Hostomska, Z. Structure-Function Analysis of the Mammalian DNA Polymerase Beta Active Site: Role of Aspartic Acid 256, Arginine 254, and Arginine 258 in Nucleotidyl Transfer. *Biochemistry* **1995**, *34*, 15934–15942. [[CrossRef](#)]
20. Brookes, A.J. The Essence of SNPs. *Gene* **1999**, *234*, 177–186. [[CrossRef](#)]
21. Hall, J.; Marcel, V.; Bolin, C.; Fernet, M.; Tartier, L.; Vaslin, L.; Hainaut, P. The Associations of Sequence Variants in DNA-Repair and Cell-Cycle Genes with Cancer Risk: Genotype-Phenotype Correlations. *Biochem. Soc. Trans.* **2009**, *37*, 527–533. [[CrossRef](#)]
22. Starcevic, D.; Dalal, S.; Sweasy, J.B. *Is There a Link between DNA Polymerase  $\beta$  and Cancer?* Taylor and Francis Inc.: Abingdon, UK, 2004; Volume 3, pp. 998–1001.
23. Kládova, O.A.; Fedorova, O.S.; Kuznetsov, N.A. The Role of Natural Polymorphic Variants of DNA Polymerase  $\beta$  in DNA Repair. *Int. J. Mol. Sci.* **2022**, *23*, 2390. [[CrossRef](#)]
24. Murphy, D.L.; Donigan, K.A.; Jaeger, J.; Sweasy, J.B. The E288K Colon Tumor Variant of DNA Polymerase  $\beta$  Is a Sequence Specific Mutator. *Biochemistry* **2012**, *51*, 5269–5275. [[CrossRef](#)] [[PubMed](#)]
25. Alnajjar, K.S.; Garcia-Barboza, B.; Negahbani, A.; Nakhjiri, M.; Kashemirov, B.; McKenna, C.; Goodman, M.F.; Sweasy, J.B. A Change in the Rate-Determining Step of Polymerization by the K289M DNA Polymerase  $\beta$  Cancer-Associated Variant. *Biochemistry* **2017**, *56*, 2096. [[CrossRef](#)]
26. Batra, V.K.; Alnajjar, K.S.; Sweasy, J.B.; McKenna, C.E.; Goodman, M.F.; Wilson, S.H. Revealing an Internal Stabilization Deficiency in the DNA Polymerase  $\beta$  K289M Cancer Variant through the Combined Use of Chemical Biology and X-ray Crystallography. *Biochemistry* **2020**, *59*, 955–963. [[CrossRef](#)] [[PubMed](#)]
27. Lang, T.; Dalal, S.; Chikova, A.; DiMaio, D.; Sweasy, J.B. The E295K DNA Polymerase Beta Gastric Cancer-Associated Variant Interferes with Base Excision Repair and Induces Cellular Transformation. *Mol. Cell Biol.* **2007**, *27*, 5587–5596. [[CrossRef](#)] [[PubMed](#)]
28. Yang, L.; Beard, W.A.; Wilson, S.H.; Broyde, S.; Schlick, T. Highly Organized but Pliant Active Site of DNA Polymerase  $\beta$ : Compensatory Mechanisms in Mutant Enzymes Revealed by Dynamics Simulations and Energy Analyses. *Biophys. J.* **2004**, *86*, 3392–3408. [[CrossRef](#)] [[PubMed](#)]
29. Murphy, D.L.; Jaeger, J.; Sweasy, J.B. A Triad Interaction in the Fingers Subdomain of DNA Polymerase Beta Controls Polymerase Activity. *J. Am. Chem. Soc.* **2011**, *133*, 6279. [[CrossRef](#)] [[PubMed](#)]
30. Skandalis, A.; Loeb, L.A. Enzymatic Properties of Rat DNA Polymerase  $\beta$  Mutants Obtained by Randomized Mutagenesis. *Nucleic Acids Res.* **2001**, *29*, 2418–2426. [[CrossRef](#)] [[PubMed](#)]

31. Maciejewski, M.W.; Liu, D.; Prasad, R.; Wilson, S.H.; Mullen, G.P. Backbone Dynamics and Refined Solution Structure of the N-Terminal Domain of DNA Polymerase Beta. Correlation with DNA Binding and DRP Lyase Activity. *J. Mol. Biol.* **2000**, *296*, 229–253. [[CrossRef](#)] [[PubMed](#)]
32. Kladova, O.A.; Tyugashev, T.E.; Mikushina, E.S.; Soloviev, N.O.; Kuznetsov, N.A.; Novopashina, D.S.; Kuznetsova, A.A. Human Pol $\beta$ ; Natural Polymorphic Variants G118V and R149I Affects Substate Binding and Catalysis. *Int. J. Mol. Sci.* **2023**, *24*, 5892. [[CrossRef](#)]
33. Micsonai, A.; Bulyáki, É.; Kardos, J. BeStSel: From Secondary Structure Analysis to Protein Fold Prediction by Circular Dichroism Spectroscopy. *Methods Mol. Biol.* **2021**, *2199*, 175–189. [[CrossRef](#)]
34. Micsonai, A.; Moussong, É.; Wien, F.; Boros, E.; Vadász, H.; Murvai, N.; Lee, Y.H.; Molnár, T.; Réfrégiers, M.; Goto, Y.; et al. BeStSel: Webserver for Secondary Structure and Fold Prediction for Protein CD Spectroscopy. *Nucleic Acids Res.* **2022**, *50*, W90–W98. [[CrossRef](#)] [[PubMed](#)]
35. Micsonai, A.; Wien, F.; Bulyáki, É.; Kun, J.; Moussong, É.; Lee, Y.H.; Goto, Y.; Réfrégiers, M.; Kardos, J. BeStSel: A Web Server for Accurate Protein Secondary Structure Prediction and Fold Recognition from the Circular Dichroism Spectra. *Nucleic Acids Res.* **2018**, *46*, W315–W322. [[CrossRef](#)] [[PubMed](#)]
36. Dunlap, C.A.; Tsai, M.D. Use of 2-Aminopurine and Tryptophan Fluorescence as Probes in Kinetic Analyses of DNA Polymerase  $\beta$ . *Biochemistry* **2002**, *41*, 11226–11235. [[CrossRef](#)]
37. Gridley, C.L.; Rangarajan, S.; Firbank, S.; Dalal, S.; Sweasy, J.B.; Jaeger, J. Structural Changes in the Hydrophobic Hinge Region Adversely Affect the Activity and Fidelity of the I260Q Mutator DNA Polymerase  $\beta$ . *Biochemistry* **2013**, *52*, 4422–4432. [[CrossRef](#)]
38. Freudenthal, B.D.; Beard, W.A.; Shock, D.D.; Wilson, S.H. Observing a DNA Polymerase Choose Right from Wrong. *Cell* **2013**, *154*, 157. [[CrossRef](#)] [[PubMed](#)]
39. Bayly, C.I.; Merz, K.M.; Ferguson, D.M.; Cornell, W.D.; Fox, T.; Caldwell, J.W.; Kollman, P.A.; Cieplak, P.; Gould, I.R.; Spellmeyer, D.C. A Second Generation Force Field for the Simulation of Proteins, Nucleic Acids, and Organic Molecules. *J. Am. Chem. Soc.* **1995**, *117*, 5179–5197. [[CrossRef](#)]
40. Zgarbová, M.; Šponer, J.; Otyepka, M.; Cheatham, T.E.; Galindo-Murillo, R.; Jurečka, P. Refinement of the Sugar-Phosphate Backbone Torsion Beta for AMBER Force Fields Improves the Description of Z- and B-DNA. *J. Chem. Theory Comput.* **2015**, *11*, 5723–5736. [[CrossRef](#)]
41. Maier, J.A.; Martinez, C.; Kasavajhala, K.; Wickstrom, L.; Hauser, K.E.; Simmerling, C. Ff14SB: Improving the Accuracy of Protein Side Chain and Backbone Parameters from Ff99SB. *J. Chem. Theory Comput.* **2015**, *11*, 3696–3713. [[CrossRef](#)]
42. Webb, B.; Sali, A. Protein Structure Modeling with MODELLER. In *Methods in Molecular Biology*; Springer: Berlin/Heidelberg, Germany, 2014; Volume 1137. [[CrossRef](#)]
43. Jurrus, E.; Engel, D.; Star, K.; Monson, K.; Brandi, J.; Felberg, L.E.; Brookes, D.H.; Wilson, L.; Chen, J.; Liles, K.; et al. Improvements to the APBS Biomolecular Solvation Software Suite. *Protein Sci.* **2018**, *27*, 112–128. [[CrossRef](#)]
44. Olsson, M.H.M.; SØndergaard, C.R.; Rostkowski, M.; Jensen, J.H. PROPKA3: Consistent Treatment of Internal and Surface Residues in Empirical PKa Predictions. *J. Chem. Theory Comput.* **2011**, *7*, 525–537. [[CrossRef](#)]
45. Jorgensen, W.L.; Chandrasekhar, J.; Madura, J.D.; Impey, R.W.; Klein, M.L. Comparison of Simple Potential Functions for Simulating Liquid Water. *J. Chem. Phys.* **1998**, *79*, 926. [[CrossRef](#)]
46. Joung, I.S.; Cheatham, T.E. Determination of Alkali and Halide Monovalent Ion Parameters for Use in Explicitly Solvated Biomolecular Simulations. *J. Phys. Chem. B* **2008**, *112*, 9020–9041. [[CrossRef](#)] [[PubMed](#)]
47. Jiang, Y.; Zhang, H.; Tan, T. Rational Design of Methodology-Independent Metal Parameters Using a Nonbonded Dummy Model. *J. Chem. Theory Comput.* **2016**, *12*, 3250–3260. [[CrossRef](#)]
48. Meagher, K.L.; Redman, L.T.; Carlson, H.A. Development of Polyphosphate Parameters for Use with the AMBER Force Field. *J. Comput. Chem.* **2003**, *24*, 1016–1025. [[CrossRef](#)]
49. Vanqualef, E.; Simon, S.; Marquant, G.; Garcia, E.; Klimerak, G.; Delepine, J.C.; Cieplak, P.; Dupradeau, F.Y. R.E.D. Server: A Web Service for Deriving RESP and ESP Charges and Building Force Field Libraries for New Molecules and Molecular Fragments. *Nucleic Acids Res.* **2011**, *39*, W511–W517. [[CrossRef](#)] [[PubMed](#)]
50. Da Silva, A.W.S.; Vranken, W.F. ACPYPE-AnteChamber PYthon Parser InterfacE. *BMC Res. Notes* **2012**, *5*, 367. [[CrossRef](#)]
51. Wennberg, C.L.; Murtola, T.; Hess, B.; Lindahl, E. Lennard-Jones Lattice Summation in Bilayer Simulations Has Critical Effects on Surface Tension and Lipid Properties. *J. Chem. Theory Comput.* **2013**, *9*, 3527–3537. [[CrossRef](#)]
52. Hess, B.; Bekker, H.; Berendsen, H.J.C.; Fraaije, J.G.E.M. LINCS: A Linear Constraint Solver for Molecular Simulations. *J. Comput. Chem.* **1997**, *18*, 1463–1472.
53. Bussi, G.; Donadio, D.; Parrinello, M. Canonical Sampling through Velocity Rescaling. *J. Chem. Phys.* **2007**, *126*, 014101. [[CrossRef](#)]
54. Bernetti, M.; Bussi, G. Pressure Control Using Stochastic Cell Rescaling. *J. Chem. Phys.* **2020**, *153*, 114107. [[CrossRef](#)]
55. Kladova, O.A.; Tyugashev, T.E.; Mikushina, E.S.; Kuznetsov, N.A.; Novopashina, D.S.; Kuznetsova, A.A. The Activity of Natural Polymorphic Variants of Human DNA Polymerase  $\beta$  Having an Amino Acid Substitution in the Transferase Domain. *Cells* **2023**, *12*, 1300. [[CrossRef](#)] [[PubMed](#)]
56. Prasad, R.; Beard, W.A.; Wilson, S.H. Studies of Gapped DNA Substrate Binding by Mammalian DNA Polymerase Beta. Dependence on 5'-Phosphate Group. *J. Biol. Chem.* **1994**, *269*, 18096–18101. [[CrossRef](#)] [[PubMed](#)]

57. Guo, Z.; Zheng, L.; Dai, H.; Zhou, M.; Xu, H.; Shen, B. Human DNA Polymerase  $\beta$  Polymorphism, Arg137Gln, Impairs Its Polymerase Activity and Interaction with PCNA and the Cellular Base Excision Repair Capacity. *Nucleic Acids Res.* **2009**, *37*, 3431–3441. [[CrossRef](#)] [[PubMed](#)]
58. Beard, W.A.; Wilson, S.H. Structure and Mechanism of DNA Polymerase  $\beta$ . *Biochemistry* **2014**, *53*, 2768–2780. [[CrossRef](#)] [[PubMed](#)]
59. Rachofsky, E.L.; Osman, R.; Ross, J.B.A.A. Probing Structure and Dynamics of DNA with 2-Aminopurine: Effects of Local Environment on Fluorescence<sup>†</sup>. *Biochemistry* **2001**, *40*, 946–956. [[CrossRef](#)] [[PubMed](#)]
60. Jean, J.M.; Hall, K.B. 2-Aminopurine Fluorescence Quenching and Lifetimes: Role of Base Stacking. *Proc. Natl. Acad. Sci. USA* **2001**, *98*, 37–41. [[CrossRef](#)]
61. Bharill, S.; Sarkar, P.; Ballin, J.D.; Gryczynski, I.; Wilson, G.M.; Gryczynski, Z. Fluorescence Intensity Decays of 2-Aminopurine Solutions: Lifetime Distribution Approach. *Anal. Biochem.* **2008**, *377*, 141–149. [[CrossRef](#)]
62. Ghisaidoobe, A.B.T.; Chung, S.J. Intrinsic Tryptophan Fluorescence in the Detection and Analysis of Proteins: A Focus on Förster Resonance Energy Transfer Techniques. *Int. J. Mol. Sci.* **2014**, *15*, 22518–22538. [[CrossRef](#)]

**Disclaimer/Publisher’s Note:** The statements, opinions and data contained in all publications are solely those of the individual author(s) and contributor(s) and not of MDPI and/or the editor(s). MDPI and/or the editor(s) disclaim responsibility for any injury to people or property resulting from any ideas, methods, instructions or products referred to in the content.